ASCE

Column Curves for Stainless Steel Lipped–Channel Sections

Jelena Dobrić, Ph.D.[1]; and Barbara Rossi, Ph.D.[2]

Abstract: The strength of thin-walled stainless steel columns has been investigated extensively over the last few years. The present paper presents the results of an extensive computational study of the buckling strength of lipped–channel section columns made of austenitic, duplex, and ferritic grades. The numerically computed strengths together with the available experimental data collected in the literature are compared to the current European and Australian/New Zealand standard (AS/NZS) codified predictions over the whole slenderness range. Minor and major axis buckling as well as flexural-torsional buckling are considered. A reliability assessment in the sense of both standards is then performed. The safety factor γ_m and resistance factor ϕ_c are computed per family of stainless steel. In conclusion, we advise the use of different European buckling column curves rather than the one currently adopted in the code and to make a distinction between the families of stainless steel. Besides, seeing the very good agreement found against the AS/NZS guidance, we propose that the factor η, currently being a linear expression in the European standard, be replaced by the AS/NZS expression with the proposed parameters for each stainless steel family. **DOI: 10.1061/(ASCE)ST.1943-541X.0002708.** *© 2020 American Society of Civil Engineers.*

PROOF ONLY

Introduction to the Design of Stainless Steel Thin-Walled Section Columns

Stainless steel is a steel alloy that contains more than 10.5% of chromium. The chromium content in mass ranges from 10.5% to 30%. Depending on the chemical composition, four families of stainless steel exist: martensitic, ferritic, austenitic, and austeno-ferritic (duplex). Their physical, chemical, and mechanical properties vary with the family, but each of them is characterized by the ability of forming a self-repairing protective oxide film providing corrosion resistance. The higher the chromium content, the more the corrosion and oxidation resistance is increased. Stainless steel is perceived as a highly decorative material, which is durable and easily maintained as well as very expensive. In the construction domain, austenitic grades were mainly used as cladding (inside or outside) thanks to their aesthetic expression. But other grades, such as duplex ones, are increasingly used in structures, as load-carrying element, thanks to the recognition of their mechanical properties combined with corrosion resistance. Fig. 1 depicts the stress-strain behavior of the families of stainless steel used in the construction domain. Typical stress-strain curves follow a nonlinear path with gradual yielding and a large strain hardening domain. Duplex types, presenting a microstructure made of austenite and ferrite, share the properties of both families and are mechanically stronger than either ferritic or austenitic types.

A substantial volume of research has been carried out over the last decades demonstrating that the response of thin-walled sections is strongly affected by local instability. Applicable design codes like the Australian/New Zealand standard (AS/NZS) 4673:2001 (AS/NZS 2001) and the European standard EN 1993-1-4 (CEN 2015) in conjunction with EN 1993-1-3 (CEN 2004) usually require the design strength to be calculated according to the effective width approach for Class 4 sections in which the cross-section capacity is based on local plate instability. In this approach, the walls are assumed to lose part of their efficiency because of local buckling. This is accounted for by a reduction of their width according to the wall element plate buckling coefficient (varying with the support conditions of the wall and the loading conditions) and on the basis of plate buckling strength curves.

The European design rules for the calculation of the cross-section capacity of thin-walled stainless steel sections are very similar to those for carbon steel but prescribe more conservative plate buckling strength curves to allow for stainless steel material nonlinearity. The reduction factor ρ to compute the effective cross-section properties may be calculated as follows:

- Internal compression elements (cold formed or welded)

$$\rho = \frac{0.772}{\bar{\lambda}_p} - \frac{0.079}{\bar{\lambda}_p^2} \quad \text{but} \quad \leq 1.0 \tag{1}$$

- Outstand compression elements (cold formed or welded)

$$\rho = \frac{1}{\bar{\lambda}_p} - \frac{0.188}{\bar{\lambda}_p^2} \quad \text{but} \quad \leq 1.0 \tag{2}$$

where $\bar{\lambda}_p$ = element slenderness defined as

$$\bar{\lambda}_p = \frac{\bar{b}/t}{28,4\varepsilon\sqrt{k_\sigma}} \tag{3}$$

where t = relevant thickness; k_σ = buckling factor corresponding to the stress ratio ψ; $\bar{b}$ = relevant flat element width; and ε = material factor equal to $\varepsilon = [(235/f_y)(E/210{,}000)]^{0,5}$ for stainless steel.

The plate strength equations of the Australian/New Zealand standard are identical with those of the ASCE standard and similar to those provided in the cold-formed carbon steel codes, with the

[1]Associate Professor, Faculty of Civil Engineering, Univ. of Belgrade, Bulevar kralja Aleksandra 73, 11000 Belgrade, Serbia. ORCID: https://orcid.org/0000-0003-1001-9154. Email: jelena@imk.grf.bg.ac.rs

[2]Associate Professor, Dept. of Engineering Science, Univ. of Oxford, Parks Rd., Oxford OX1 3PJ, UK; Dept. of Civil Engineering, Katholieke Universiteit Leuven, 3000 Leuven, Belgium (corresponding author). ORCID: https://orcid.org/0000-0001-6228-0309. Email: barbara.rossi@new.ox.ac.uk; barbara.rossi@kuleuven.be

Note. This manuscript was submitted on April 4, 2019; approved on February 19, 2020No Epub Date. Discussion period open until 0, 0; separate discussions must be submitted for individual papers. This paper is part of the ***Journal of Structural Engineering***, © ASCE, ISSN 0733-9445.

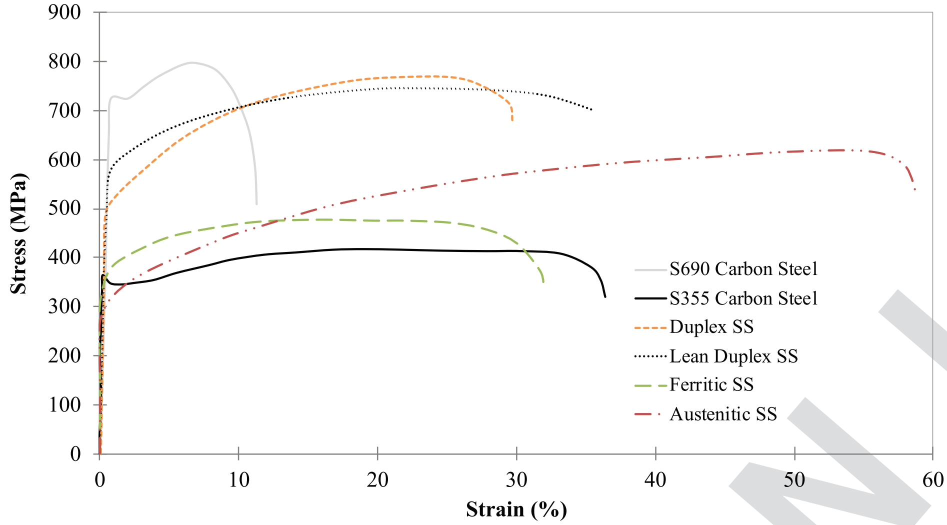

F1:1 **Fig. 1.** Typical stress-strain curves for austenitic, ferritic, and duplex/lean duplex stainless steel compared to S355 and S690 carbon steel.

plate buckling curve for uniformly compressed elements being Winter's equation.

The effects of distortional buckling should be allowed for lipped–channel cross-sections. In the present study, the procedure suggested in EN 1993-1-3 Clause 5.5.1(5) (CEN 2004) was used when necessary.

The current version of the European design rules does not allow the enhanced corner properties to be utilized through the average cross-section yield strength unless the section is fully effective. However, for stainless steel sections, the work-hardening associated with cold forming operations during fabrication generally greatly increases the cross–sectional resistance. A method was developed and recently published in the 4th edition of the *Design Manual for Structural Stainless Steel* (Afshan et al. 2017) to account for the beneficial effects of work hardening. The method is based on Rossi et al. (2013) in which lipped–channel cross-sections were also included, which is especially important to take that into account for columns in the low slenderness range.

To obtain the member buckling resistance, two general approaches can be considered:

- The tangent stiffness method. In order to account for the nonlinear stress-strain curve of stainless steel, the specifications replace the initial elastic modulus by the tangent modulus E_t corresponding to the buckling stress. Adopted in the American and Australian/New Zealand codes, the tangent stiffness method is based on the Euler formula and is an iterative method.
- The Perry-Robertson method. The European code proposes a noniterative method in which different curves based on the Perry-Robertson buckling curve are provided for various cross-sections, accounting for differences in terms of the initial geometric imperfection and manufacturing process (cold-formed or welded for stainless steel members). The current version of the European code does not account for differences in mechanical properties between different alloys.

To obtain the flexural buckling (FB) resistance of a stainless steel column, Eqs. (4) and (5) are provided in the Eurocode

$$N_{b,Rd} = \chi A f_y/\gamma_{M1} \quad \text{for Class 1, 2, and 3 cross-sections} \tag{4}$$

$$N_{b,Rd} = \chi A_{\text{eff}} f_y/\gamma_{M1} \quad \text{for Class 4 cross-sections} \tag{5}$$

where χ = reduction factor for the relevant buckling mode; A = gross cross-sectional area; and A_{eff} = effective cross-sectional area.

The reduction factor to account for flexural buckling is provided by Eq. (6)

$$\chi = \frac{1}{\phi + [\phi^2 - \bar{\lambda}^2]^{0.5}} \leq 1.0 \tag{6}$$

where

$$\phi = 0,5(1 + \alpha(\bar{\lambda} - \bar{\lambda}_0) + \bar{\lambda}^2) \tag{7}$$

$$\bar{\lambda} = \sqrt{\frac{A f_y}{N_{cr}}} = \frac{L_{cr}}{i}\frac{1}{\pi}\sqrt{\frac{f_y}{E}} \quad \text{for Class 1, 2, and 3 cross-sections} \tag{8}$$

$$\bar{\lambda} = \sqrt{\frac{A_{\text{eff}} f_y}{N_{cr}}} = \frac{L_{cr}}{i}\frac{1}{\pi}\sqrt{\frac{f_y \frac{A_{\text{eff}}}{A}}{E}} \quad \text{for Class 4 cross-sections} \tag{9}$$

where α = imperfection factor; N_{cr} = elastic critical force for the relevant buckling mode based on the gross cross sectional properties; $\bar{\lambda}_0$ = limiting nondimensional slenderness; L_{cr} = buckling length in the buckling plane considered; and i = radius of gyration about the relevant axis, determined using the properties of the gross cross-section.

Slightly altered formulas apply to torsional and flexural-torsional buckling and can be found in EN 1993-1-3 (CEN 2004).

The parameters α and $\bar{\lambda}_0$ currently depend only on the buckling mode and type of member (cold-formed open sections, hollow sections, and welded open sections). Table 1 provides the values currently used in Eurocode for all types of members and buckling modes. Nevertheless, the experimental research over the last 10 years has shown that the EN 1993-1-4 buckling curves for cold formed hollow sections are optimistic and that there is a difference in buckling behavior among the stainless steel family as, for example, between ferritic stainless steel cold formed rectangular hollow section columns compared to austenitic and duplex stainless steels.

The present paper gives evidence that the same conclusion can be drawn for cold formed lipped-channels and that the parameters α and $\bar{\lambda}_0$ currently adopted in EN 1993-1-4, which are respectively equal to 0.49 and 0.4, should be revised. The updated buckling curves (Table 2) have already been published in the 4th edition of

PROOF ONLY

Table 1. Imperfection factor α and limiting slenderness $\bar{\lambda}_0$

	Type of buckling	Type of member	α	$\bar{\lambda}_0$
T1:1	Type of buckling	Type of member	α	$\bar{\lambda}_0$
T1:2	Flexural	Cold formed open sections	0.49	0.40
T1:3	Flexural	Hollow sections (welded and seamless)	0.49	0.40
T1:4	Flexural	Welded open sections (major axis)	0.49	0.20
T1:5	Flexural	Welded open sections (minor axis)	0.76	0.20
T1:6	Torsional and flexural-torsional	All members	0.34	0.20

Source: Data from CEN (2015).

Table 2. Updated values of the imperfection factor α and limiting slenderness $\bar{\lambda}_0$

			Austenitic and duplex		Ferritic	
T2:1 T2:2	Type of member	Axis of buckling	α	$\bar{\lambda}_0$	α	$\bar{\lambda}_0$
T2:3	Cold formed angles and channels	Any	0.76	0.2	0.76	0.2
T2:4	Cold formed lipped-channels	Any	0.49	0.2	0.49	0.2
T2:5	Cold formed RHS	Any	0.49	0.3	0.49	0.2
T2:6	Cold formed CHS/EHS	Any	0.49	0.2	0.49	0.2
T2:7	Hot finished RHS	Any	0.49	0.2	0.34	0.2
T2:8	Hot finished CHS/EHS	Any	0.49	0.2	0.34	0.2
T2:9	Welded or hot-rolled open	Major	0.49	0.2	0.49	0.2
T2:10	sections	Minor	0.76	0.2	0.76	0.2

Note: RHS = rectangular hollow section; CHS = circular hollow section; and EHS = elliptical hollow section.
Source: Data from Afshan et al. (2017).

the *Design Manual for Structural Stainless Steel* (Afshan et al. 2017), and it is expected that the next revision to EN 1993-1-4 will give these new flexural buckling curves.

Local buckling of slender monosymmetric cross-section causes a shift of the centroid of the effective cross-section, which consequently introduces a secondary bending moment. Therefore, an initially centrically compressed column becomes a beam-column. The effective width approach for local-overall interaction account for effective section properties in the calculation of the beam-column buckling stress. For a stainless steel column with Class 4 cross-sections, Eqs. (10)–(12) from Clause 5.5 of EN 1993-1-4 take into account interaction effects between a compressive axial load and uniaxial bending moment induced by the shift of the effective centroid

$$\frac{N_{Ed}}{(N_{b,Rd})'} + k_y\left(\frac{N_{Ed}e_{Ny}}{W_{\text{eff},y}f_y/\gamma_{M1}}\right) \leq 1.0 \text{ to prevent premature buckling about the major axis} \quad (10)$$

$$\frac{N_{Ed}}{(N_{b,Rd})''} + k_{LT}\left(\frac{N_{Ed}e_{Ny}}{M_{b,Rd}}\right) \leq 1.0 \text{ to prevent premature buckling about the major axis for members subject to lateral-torsional buckling} \quad (11)$$

$$\frac{N_{Ed}}{(N_{b,Rd})'} + k_z\left(\frac{N_{Ed}e_{Nz}}{W_{\text{eff},z}f_y/\gamma_{M1}}\right) \leq 1.0 \text{ to prevent premature buckling about the major axis} \quad (12)$$

For axial compression and biaxial moments, all beam-column members with a slender cross-section should satisfy

$$\frac{N_{Ed}}{(N_{b,Rd})'} + k_y\left(\frac{N_{Ed}e_{Ny}}{W_{\text{eff},y}f_y/\gamma_{M1}}\right) + k_z\left(\frac{N_{Ed}e_{Nz}}{W_{\text{eff},z}f_y/\gamma_{M1}}\right) \leq 1.0 \quad (13)$$

$$\frac{N_{Ed}}{(N_{b,Rd})''} + k_{LT}\left(\frac{N_{Ed}e_{Ny}}{M_{b,Rd}}\right) + k_z\left(\frac{N_{Ed}e_{Nz}}{W_{\text{eff},z}f_y/\gamma_{M1}}\right) \leq 1.0 \quad (14)$$

where N_{Ed} = applied design value of the axial compression load; e_{Ny} and e_{Nz} = shifts of the centroidal axes when the cross-section is subject to the uniform compression; $(N_{b,Rd})'$ = smallest value of the design buckling load $N_{b,Rd}$ for the following four buckling modes: flexural buckling about the y-axis $N_{b,Rd,y}$, flexural buckling about the z-axis, torsional buckling, and torsional-flexural buckling; $(N_{b,Rd})''$= smallest value of $N_{b,Rd}$ for the following three buckling modes: flexural buckling about the z-axis, torsional buckling, and torsional-flexural buckling; and $M_{b,Rd}$ = design lateral-torsional buckling resistance. The interaction factors k_y, k_z, and k_{LT} can be calculated as follows:

$$k_y = 1.0 + 2(\bar{\lambda}_y - 0.5)\frac{N_{Ed}}{N_{b,Rd,y}} \quad \text{but} \quad 1.2 \leq k_y \leq 1.2 + 2\frac{N_{Ed}}{N_{b,Rd,y}} \quad (15)$$

$$k_z = 1.0 + 2(\bar{\lambda}_z - 0.5)\frac{N_{Ed}}{(N_{b,Rd})''} \quad \text{but} \quad 1.2 \leq k_z \leq 1.2 + 2\frac{N_{Ed}}{(N_{b,Rd})''} \quad (16)$$

$$k_{LT} = 1.0 \quad (17)$$

For cold-formed cross-sections, according to EN 1993-1-3 (CEN 2004), an alternative interaction formula [Eq. (18)] may be used

$$\left(\frac{N_{Ed}}{N_{b,Rd}}\right)^{0.8} + \left(\frac{M_{Ed}}{M_{b,Rd}}\right)^{0.8} \leq 1.0 \quad (18)$$

where M_{Ed} includes the effects of shifts of neutral axis, if relevant.

The flexural buckling resistance of a stainless steel column according to AS/NZS 4673:2001 (AS/NZS 2001) is

$$N_{\text{ce}} = \phi_c A_e f_n \quad (19)$$

where

$$\phi_c = 0,9 \quad (20)$$

$$f_n = \frac{f_y}{\phi + [\phi^2 - \bar{\lambda}^2]^{0.5}} \leq f_y \quad (21)$$

$$\phi = 0,5(1 + \eta + \bar{\lambda}^2) \quad (22)$$

$$\eta = \alpha^*((\bar{\lambda} - \bar{\lambda}_1)^\beta - \bar{\lambda}_0^*) \quad (23)$$

where the values of α^*, β, $\bar{\lambda}_0^*$, and $\bar{\lambda}_1$ shall be as given in Table 3.

Note that the parameters included in Eq. (23) do not bear the same significations as the ones in Eq. (7). The parameter η in the Australian code should be compared to $\alpha(\bar{\lambda} - \bar{\lambda}_0)$ in the European one, where $\bar{\lambda}_0$ is the limiting nondimensional slenderness. In the subsequent sections of this paper, the parameters provided in Table 3 will be denoted with the superscript * as in α^* and $\bar{\lambda}_0^*$.

PROOF ONLY

Table 3. Imperfection factors and the limiting slenderness α^*, β, $\bar{\lambda}_0^*$, and $\bar{\lambda}_1$ depending on grade

	Types		
Buckling factors	Austenitic	Ferritic EN 1.4003	Duplex
α^*	1.59	0.94	1.16
β	0.28	0.15	0.13
$\bar{\lambda}_0^*$	0.55	0.56	0.65
$\bar{\lambda}_1$	0.20	0.27	0.42

Source: Data from AS/NZS 4673:2001 (AS/NZS 2001).

These generic equations can be found in Rasmussen and Rondal (1997, 2000). The Australian specification employs Clause 3.5 with interaction expressions, as given by Eqs. (24) and (25), in which N^*, M_y^*, and M_z^* are the design axial compressive load and design bending moments about the y- and z-axis of the effective section, respectively; N_c is the nominal buckling capacity of the centrically compressed member; M_{by} and M_{by} are the nominal bending member capacity about the y- and z-axis, respectively; N_s is the nominal cross-section capacity of the centrically compressed member; α_{ny} and α_{nz} are the amplification factors equal to $(1 - N^*/N_e)$; C_{my} and C_{mz} are the equivalent uniform moment factors, which are equal to unity for members with a constant first order bending moment along their length and for members whose ends are unrestrained; and ϕ_c and ϕ_b are the strength reduction factors for compression and bending, respectively

$$\frac{N^*}{\phi_c N_c} + \frac{C_{my} M_y^*}{\phi_b M_{by} \alpha_{ny}} + \frac{C_{mz} M_z^*}{\phi_b M_{bz} \alpha_{nz}} \leq 1.0 \tag{24}$$

$$\frac{N^*}{\phi_c N_s} + \frac{M_y^*}{\phi_b M_{by}} + \frac{\mathrm{M}_z^*}{\phi_b M_{bz}} \leq 1.0 \tag{25}$$

Reference Experimental and Numerical Results

In the present study, the experimental and numerically computed ultimate loads published by different authors in the literature were collected and analyzed.

In Kuwamura (2003), lipped–channel cross-sections made of the stainless steel grades EN 1.4301 and EN 1.4003 were tested. In total, 4 channel and 11 lipped–channel sections were tested. Dobrić et al. (2017) performed four repeated tests on plain channel sections made of the grade EN1.4301. In the studies by Lecce (2006) and Lecce and Rasmussen (2004, 2006), a total of 19 tests were performed, including 11 simple lipped–channel columns and 8 lipped–channel columns with intermediate stiffeners made of EN1.4301, EN1.4016, and EN1.4003. Additionally, Becque et al. (2008) performed a total of 36 and 24 tests on lipped–channel columns and I-section columns, respectively. The I-section columns consisted of two back-to-back plain channels interconnected by screws. In the study by Becque and Rasmussen (2009a, b), 29 lipped–channel columns made of EN1.4003, EN1.4301, and EN 1.4016 were tested. In studies by Schepens (2008) and Rossi et al. (2010), 21 lipped–channel columns made of EN1.4003 were considered. In the previously cited references, several FE models were also calibrated against tests, and parametric studies were conducted. Those experiments along the numerical values of the ultimate loads for the flexural buckling of channel section columns are included in the present study. The theoretical buckling loads were also recalculated based on the recommendations of EN 1993-1-3 and EN 1993-1-4, as mentioned in the introduction.

Numerical Study

Calibration of the Finite-Element Model

A detailed finite-element analysis (FEA) was carried out to simulate the experiments of Rossi et al. (2010) and Lecce and Rasmussen (2004, 2006) and to identify the key factors affecting the buckling response. A quasi-static analysis was carried out with the Abaqus software package (version 6.12), employing its explicit dynamic solver because it was already successfully used for simulations of column buckling tests (Dobrić et al. 2018). Two types of numerical analyses were performed for each FE model: an eigenvalue linear bifurcation analysis and a geometrically and materially nonlinear buckling analysis.

In order to model the experiment of Rossi et al. (2010), the measured geometry was modeled using S4R shell elements with reduced integration and finite membrane strain. A square element with a size of 2 mm (approximately equal to 1.5 times the cross-section thickness) was used to discretize the flat and corner parts of the modeled cross-section. To model the supporting conditions of the specimens during the tests, the end plates of the testing machine were modeled as two-dimensional (2D) rigid bodies. Four solid elements were introduced to simulate the guiding plates placed along the outside and inside cross-section perimeters during the experiment. Contact conditions between the guiding plates and the end-plates of the testing machine were defined through tie constraints on the joining surfaces. The surface-to-surface general contact was selected to take into account the interactions between the surfaces of the end cross-sections and the guiding plates. Two reference points were set at the centroid of the top and bottom bearing plates. Loading until failure was applied as displacement was controlled. Typical geometry of the boundary conditions and the mesh of the model of these tests are shown in Fig. 2(a).

In Rossi et al. (2010), the base material is the ferritic stainless steel alloy EN1.4003. The analytical stress-strain curves for the flat and corner parts of the press-braked section were defined by employing a modified Ramberg-Osgood material model according to Arrayago et al. (2015). A strength enhancement due to work hardening in the corner parts of the cross-section was considered according to the predictive model of Rossi et al. (2013). The analytical stress-strain curves were transformed to the true stress-strain curves to be inputted in the Abaqus stress-strain plasticity model (Fig. 3). Plasticity with isotropic hardening was used with a modulus of elasticity, $E = 200{,}000\ \mathrm{N/mm^2}$, and Poisson's ratio, $v = 0.3$.

Geometric imperfections were considered by incorporating the shapes of the eigenmode displacements obtained via a linear bifurcation analysis. The geometric imperfections were assigned to the FE models as linear combinations of wave sine functions, which reflect the linear bifurcation analysis mode-shapes. Four shape distributions of geometric imperfections were considered: a sine wave (bow) imperfection in the plane perpendicular to the minor principal axis, a twist imperfection, a local imperfection, and a distortional geometric imperfection. The imperfection amplitudes were the measured ones. The residual stresses induced by the cold working process were not included in the FE models, considering their insignificant effect on the overall behavior of the compressed members (Rasmussen and Hancock 1993; Gardner and Nethercot 2004).

Ten FE models with different lengths were modeled. In sum, the average numerical-to-experimental ultimate load is 1.01 with a coefficient of variation of 1.81% (Table 4). The numerical failure modes correspond to the experimental ones. They consist of a combination of distortional buckling and minor axis flexural buckling for short columns or flexural-torsional buckling for longer

PROOF ONLY

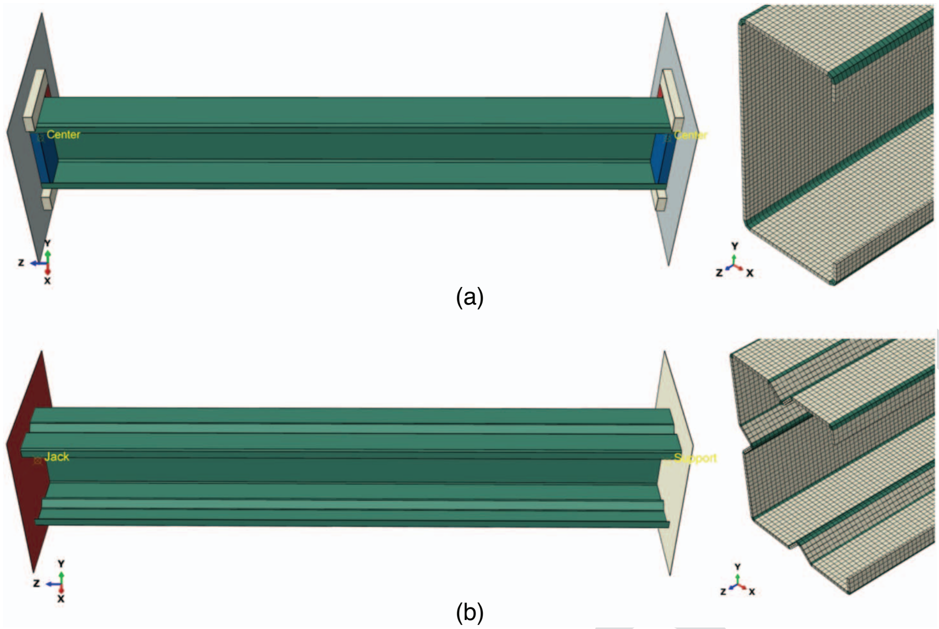

F2:1 **Fig. 2.** Geometry, boundary conditions, and mesh of the calibrated FE models.

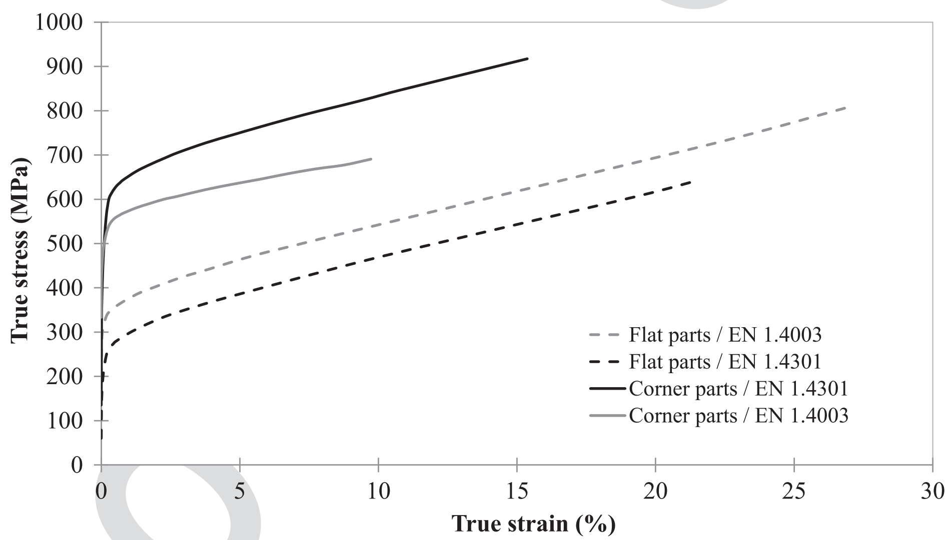

F3:1 **Fig. 3.** Stress-strain curves for the flats and corners used in the FE models by Lecce and Rasmussen (2004) and Rossi et al. (2010).

Table 4. Comparison between the failure loads in experiments by Rossi et al. (2010) and FEA

	Lengths of specimens in FE models (mm)	Repeated tests					
T4:1 T4:2		1 (kN)	2 (kN)	3 (kN)	$N_{b,u,\mathrm{exp,mean}}$ (kN)	$N_{b,u,\mathrm{FEA}}$ (kN)	$N_{b,u,\mathrm{FEA}}/N_{b,u,\mathrm{exp,mean}}$
T4:3	400	80.9	80.3	80.6	80.6	80.0	0.99
T4:4	700	80.7	81.1	78.8	80.2	80.4	1.00
T4:5	900	80.8	80.1	76.9	79.3	80.1	1.01
T4:6	1,200	78.0	78.5	77.4	78.0	77.8	1.00
T4:7	1,400	76.4	76.9	75.5	76.3	76.8	1.01
T4:8	1,800	72.7	70.7	72.3	71.9	72.3	1.01
T4:9	2,200	67.5	69.6	69.0	68.7	68.6	1.00
T4:10	2,600	65.1	61.9	59.7	62.2	62.0	1.00
T4:11	3,000	49.0	49.0	48.9	49.0	50.4	1.03
T4:12	3,200	42.8	49.6	49.0	47.1	48.3	1.02
T4:13	Mean	—	—	—	—	—	1.01
T4:14	CoV[a] (%)	—	—	—	—	—	1.81

[a]CoV means coefficient of variation.

PROOF ONLY

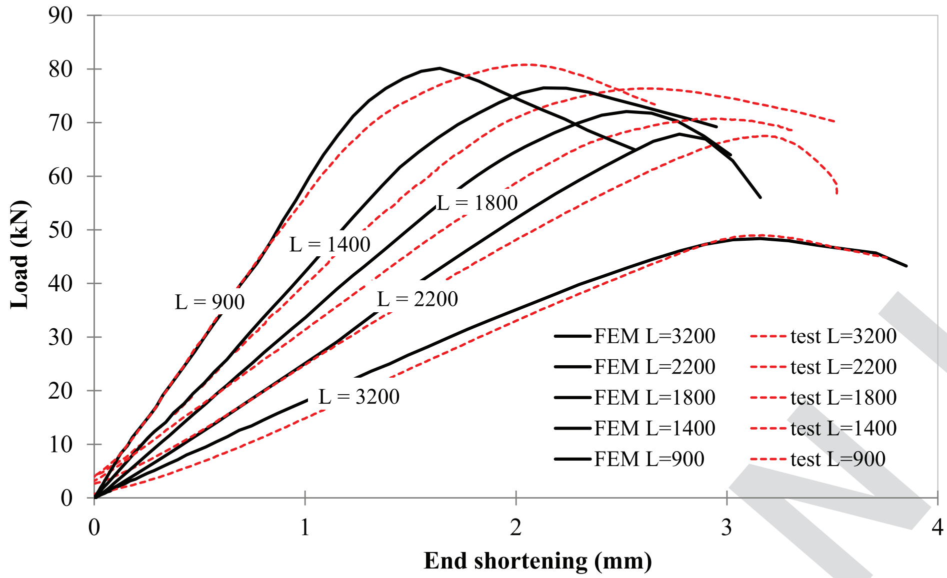

Fig. 4. Load versus end shortening recorded during some of the experiments by Rossi et al. (2010) compared to the FEA results.

columns. Good agreement was obtained between the experimental transversal cross-sectional displacements and the numerical ones. Fig. 4 provides a comparison of the load versus vertical displacement response recorded during the tests against the computed ones.

To model the experiments of Lecce and Rasmussen (2004), the same concepts were used with some exceptions: (1) the element size was 3 mm (equal to 1.5 times the cross-section thickness); and (2) the end plates of the testing machine were also modeled as 2D rigid bodies with contact conditions between the column end cross-sections and the end plates defined via the tie constraints at the joining surfaces, but there was no additional plate preventing warping of the end cross-sections. The FE model representing the column buckling test (Lecce and Rasmussen 2004) is shown in Fig. 2(b). The same procedure was used to model the corner and flat material characteristics, but the stainless steel alloy was the austenitic grade EN1.4301. The analytical stress-strain curves for the flat and corner parts of the press-braked section were defined by employing a modified Ramberg–Osgood material model, according to Arrayago et al. (2015). The key material properties were obtained through tensile flat and corner coupon tests by Lecce and Rasmussen (2004) and were used in the present FE model.

The geometric imperfections causing inward flange movement or outward flange movement were assigned to the FE models with measured amplitude provided in Lecce and Rasmussen (2004). Those amplitudes were measured at the flange-lip junction and in the center of the web and introduced likewise in the model. Four experiments were modeled. As for the previous experimental program, the average numerical-to-experimental ultimate load is 1.00 with a coefficient of variation of 0.95% (Table 5).

Table 5. Comparison between the failure loads in experiments by Lecce and Rasmussen (2004) and FEA

FE models with specimen designations as in Lecce and Rasmussen (2004)	$N_{b,u,\mathrm{exp}}$ (kN)	$N_{b,u,\mathrm{FEA}}$ (kN)	$N_{b,u,\mathrm{FEA}}/N_{b,u,\mathrm{exp}}$
304D1a/304D1b	101.5	100.8	0.99
304D2a/304D2b	104.0	103.7	1.00
304DS1a	132.0	132.8	1.01
304Ds1b	134.0	135.7	1.01
Mean	—	—	1.00
CoV (%)	—	—	0.95

Fig. 5 compares the FE load-end shortening curves with the corresponding experimental curves. Good agreement is achieved in terms of overall shape, initial stiffness, deformation capacity, and ultimate resistance. The numerical failure modes show inward or outward distortional buckling and correspond to the experimental ones.

Sensitivity Study to the Imperfection

A sensitivity study of the numerical results to several combinations of imperfection modes and amplitudes was carried out on lipped–channel section columns. The imperfection sensitivity study includes an impact assessment of the distributions and magnitudes of four different imperfections: flexural (bow), local, distortional (as in Fig. 6), and twist (torsional) deviations were considered.

The magnitude of the imperfection, based on the eigenmode analysis, was successively chosen equal to $w = \pm t$ for a leading distortional imperfection, in agreement with Schafer and Pekoz (1998); $\pm d/100$ and then $\pm d/200$ for a leading local imperfection, in accordance with the cross-section tolerance given in EN 1090-2 (CEN 2008); and $\pm d/50$ for a leading twist imperfection, based on Annex C of EN 1993-1-5 (CEN 2006). Following Clause C.5.(5) of EN 1993-1-5, one of the cross-section imperfections was taken as the leading imperfection, and the others were taken as the accompanying imperfections whose amplitudes were reduced by a factor 0.7.

First, all the mentioned cases were combined with the measured global imperfection, i.e., a sine wave geometric imperfection in the plane perpendicular to the minor principal axis with the measured amplitude. Then the same FE models were completed with a flexural imperfection with a magnitude of $\pm\delta = L/1000$. In total, 460 models were analyzed. The results of the study were compared against the experimental results of Rossi et al. (2010). Based on these comparisons, it was found that the pattern using a leading local imperfection with an amplitude of $d/100$ in the low slenderness domain, a distortional imperfection of t in the intermediate slenderness domain, and a twist imperfection of $d/50$ in the high slenderness domain leads to the best agreement with the experimental results. Depending on the slenderness domain, the accompanying three imperfections included in the pattern are reduced by 0.7.

PROOF ONLY

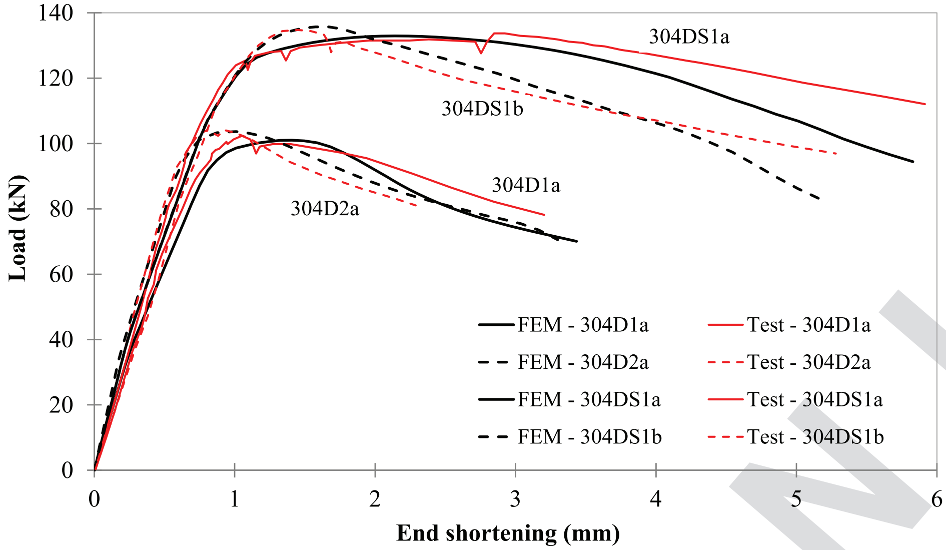

Fig. 5. Load versus end shortening recorded during the experiments by Lecce and Rasmussen (2004) compared to the FEA results.

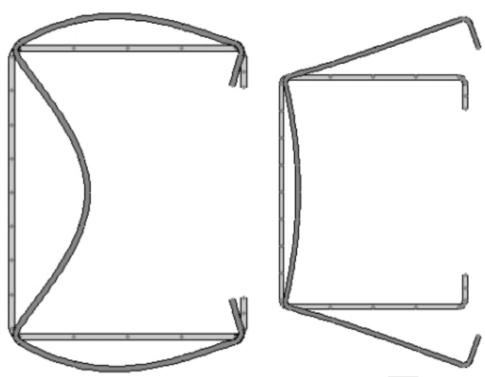

Fig. 6. Typical local and (outward) distortional buckling shape of a lipped-channel obtained from a finite strip elastic buckling analysis.

In the following parametric study, this pattern will be used together with a flexural imperfection with a magnitude of $\delta = L/1000$.

Parametric Study

Studied Grades and Stress-Strain Behavior

To conduct a reliable statistical analysis, at least 60 FE models for each stainless steel family were carried out. Three grades were included, namely EN1.4301, EN1.4162, and EN1.4003. The stress-strain behavior of the studied grades was modeled through the so-called Ramberg-Osgood material model, according to Arrayago et al. (2015). Strength enhancement due to work hardening in the corner regions of the cross-section was considered according to the predictive model of Rossi et al. (2013). Key material properties are based on Rossi et al. (2010) tests (EN1.4003), Dobrić et al. (2017) tests or Lecce and Rasmussen's (2004) tests (EN1.4301), and Saliba and Gardner's (2013) tests (EN1.4162). Columns made of cold-rolled austenitic stainless steel strips [using the material model of Dobrić et al.'s (2017) tests] have different structural responses than columns made of hot-rolled austenitic stainless steel strips [using the material model available from Lecce and Rasmussen (2004)]; therefore, both material models were included, so in total four material models were included. Tables 6 and 7 provide the material parameters included in the FE models for the flats and corners of the studied cross-sections.

Studied Geometries

The FE parametric study includes 13 different lipped–channel cross-section dimensions satisfying the conditions provided in Table 5.1 of EN 1993-1-3. Pinned-end columns were studied, addressing their flexural buckling capacity about the minor and major principal axis and flexural-torsional buckling capacity. The cross-section geometries cover the whole range of cross-section classes, with wall thicknesses ranging from 1.5 to 6 mm, as provided in Table 8, with the used dimensional code for the cross-section geometry, as provided in Fig. 7. The whole range of column slenderness is covered up to $\bar{\lambda} = 2.5$.

3 **Table 6.** Key material properties of flat cross-section parts adopted in the FE models

Stainless steel grade/source	f_y (N/mm^2)	f_u (N/mm^2)	ε_u (%)	Strain hardening parameters n	m
EN 1.4003/Rossi et al. (2010)	337	614	29	13.5	2.0
EN 1.4162/Rossi et al. (2013)	569	753	25	12.0	3.0
EN 1.4301/Lecce and Rasmussen (2004)	251	703	57	5.0	2.2
EN 1.4301/Dobrić et al. (2017)	307	634	53	6.3	2.2

PROOF ONLY

Table 7. Key material properties of corner cross-section parts adopted in the FE models

Stainless steel grade/source	f_y (N/mm^2)	f_u (N/mm^2)	ε_u (%)	Strain hardening parameters	
				n	m
EN 1.4003, Rossi et al. (2010)	525	624	10	13.5	3.4
EN 1.4162, Rossi et al. (2013)	712	813	14	12.0	3.4
EN 1.4301, Lecce and Rasmussen (2004)	570	784	16	5.0	3.0
EN 1.4301, Dobrić et al. (2017)	458	680	37	4.9	2.5

Table 8. Lipped–channel—cross-section geometries and lengths included in the present study (millimeters)

Section	Length	d	b	c	t	r_i
LC 100 × 50 × 12 × 1.5	300–3,200	100.0	50.0	12.0	1.5	2.3
LC 120 × 60 × 25 × 6	250–2,000	120.0	60.0	25.0	6.0	12.0
LC 100 × 40 × 16 × 4	300–1,800	100.0	40.0	16.0	4.0	8.0
LC 100 × 40 × 15 × 2	300–1,800	100.0	40.0	15.0	2.0	4.0
LC 150 × 82 × 30 × 4	300–3,000	150.0	82.0	30.0	4.0	8.0
LC 140 × 60 × 25 × 4	300–3,200	140.0	60.0	25.0	4.0	8.0
LC 140 × 60 × 25 × 2	300–2,800	140.0	60.0	25.0	2.0	4.0
LC 200 × 80 × 35 × 4	600–3,000	200.0	80.0	35.0	4.0	8.0
LC 160 × 90 × 25 × 4	480–3,100	160.0	90.0	25.0	4.0	8.0
LC 180 × 80 × 35 × 4	600–2,500	180.0	80.0	35.0	4.0	8.0
LC 180 × 80 × 35 × 2	600–2,800	180.0	80.0	35.0	2.0	8.0
LC 180 × 50 × 30 × 4	600–2,500	180.0	50.0	30.0	4.0	8.0
LC 180 × 50 × 30 × 2	600–2,500	180.0	50.0	30.0	2.0	8.0

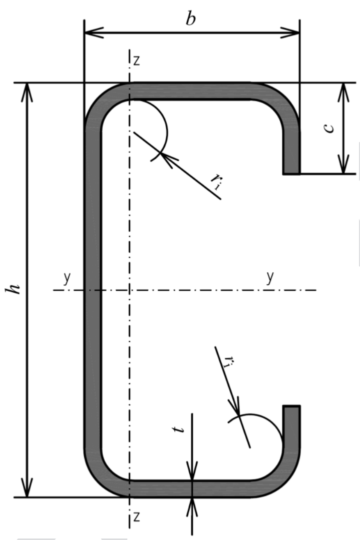

Fig. 7. Designations of cross-section geometry.

A shell element S4R with a size equal to 1.5t, where t is the cross-section thickness, was applied to discretize the whole column cross-section in the FE parametric study. The same size of shell elements was used along the length of the FE models. The end section boundary conditions of the FE models replicate pin-ended conditions about the principal axes of the cross-sections, perpendicular to the buckling planes. The reference points are set at the centroids of the column's end cross-sections and kinematically constrained with the cross-section points (node surfaces, see Fig. 8) at each column end. Displacement control was used to apply the compressive load to the reference point in the loading zone. The geometry, mesh, and boundary conditions of one typical model are presented in Fig. 8. An eigenvalue linear bifurcation analysis was employed to obtain the initial imperfection mode shapes and permit a realistic incremental nonlinear FE analysis. A superposition of the initial imperfection shapes, as described in the previous imperfection sensitivity study, was assigned to the models, carefully considering the governing cross-section buckling shapes of channel and lipped–channel columns, respectively. A geometrically and materially nonlinear analysis was performed to obtain the ultimate loads and failure modes using the dynamic explicit solver in the Abaqus software package (version 6.12).

To be able to assess the behavior of columns failing by flexural buckling about the major principal axis (which is not a dominant failure mode for lipped–channel columns), lateral restraints were added along the column length in the FE model to force this mode to occur. It is worth noting that no such restraints were added to study minor axis or flexural-torsional buckling.

Comparison with the European Buckling Curves

In total, around 900 data points are included in this study, of which about 700 are characterized by a column slenderness $\bar{\lambda}$ higher than 0.2. All the FE models were carefully analyzed to identify the failure modes. Either flexural-torsional buckling or flexural buckling about the minor axis occurred and, in the following comparison, the appropriate failure mode was chosen to evaluate the corresponding theoretical failure load. Major axis flexural buckling was obtained using appropriate boundary conditions along the column length and did not necessitate further identification. For slender cross-sections, the geometrical properties of the effective cross-sections were obtained based on the design approach from EN 1993-1-3, considering the reduction factors provided in Eqs. (1) and (2) of the *Design Manual for Structural Stainless Steel* (Afshan et al. 2017).

Different combinations of the imperfection factor α, being either 0.49 or 0.76 (buckling curve c and d in EN 1993-1-1), with the

PROOF ONLY

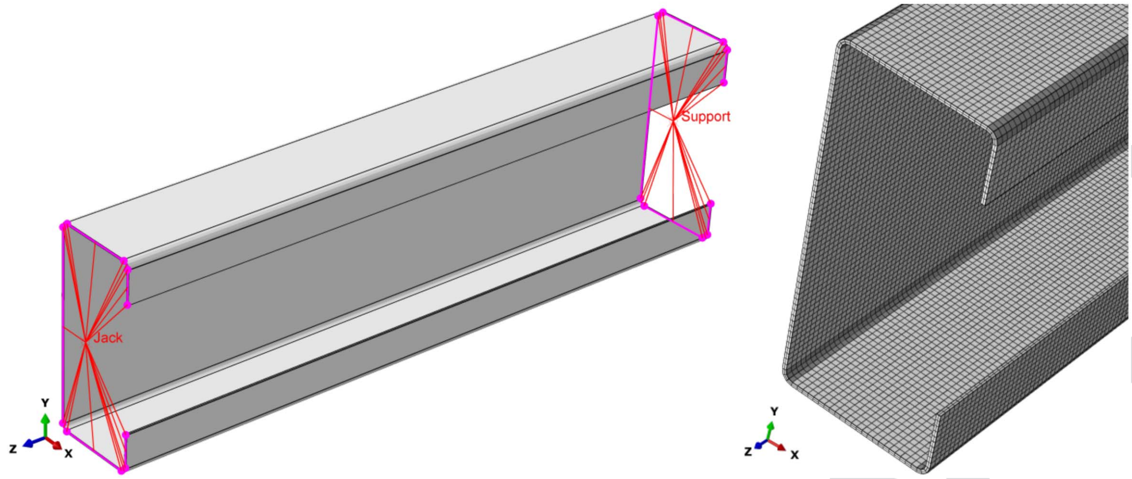

Fig. 8. Geometry and boundary conditions of one typical FE model.

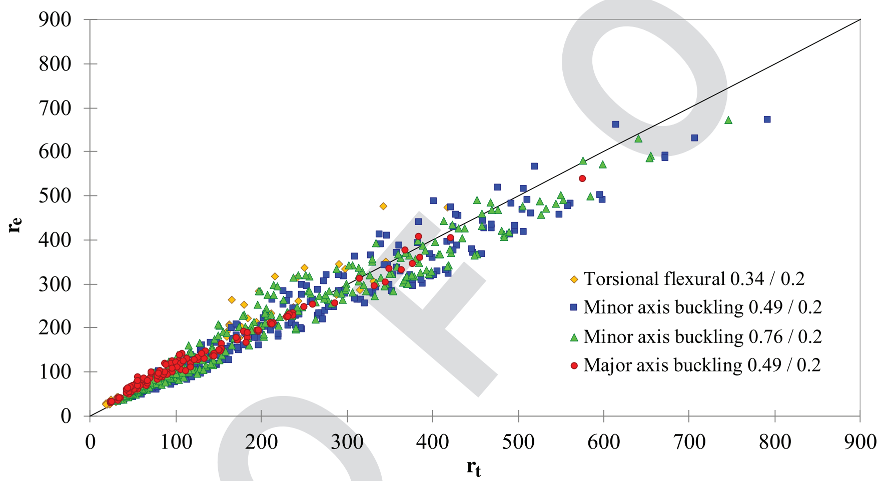

Fig. 9. Comparison of the numerically computed data with the European buckling curves for the flexural buckling of lipped–channel section columns—minor and major axis buckling as well as flexural-torsional buckling.

limiting nondimensional slenderness $\bar{\lambda}_0$ being 0.2, were considered to predict the flexural buckling loads. It is worth recalling that $\alpha = 0.49$ and $\bar{\lambda}_0 = 0.2$ are the values proposed in *Design Manual for Structural Stainless Steel* (Afshan et al. 2017) for lipped-channels. Note that this modification also affects the flexural-torsional buckling load. When the slenderness is smaller than 0.2, the highest effect of work hardening takes place, and the buckling effects may be ignored for these points. The buckling Curve b ($\alpha = 0.34$ and $\bar{\lambda}_0 = 0.2$) was used to predict the flexural-torsional buckling loads. Fig. 9 compares the theoretical resistance values $r_{t,i}$ using the present resistance function, based on the measured material and geometric properties, with the experimental resistance values $r_{e,i}$ from each test i or FE model.

For flexural buckling and flexural-torsional buckling of lipped–channel section columns, the limiting nondimensional slenderness appears to be close to 0.2 while the global imperfection factor for the slenderness higher than about 0.6 is closer to 0.49 as indicated in *Design Manual for Structural Stainless Steel* (Afshan et al. 2017).

The scatter of the data is higher for the flexural-torsional buckling mode [although based on a fewer amount of data points (Table 9)] than for the flexural mode and shows, for the slenderness above 1.0, a higher level of conservativeness of the codified predictions.

The AS/NZS standard, which considers the difference in the stress-strain diagram of each stainless steel family via the values of α^*, β, $\bar{\lambda}_0^*$, and $\bar{\lambda}_1$, as provided in Table 3, provides slightly better predictions as well as lower scatter. However, as seen in Fig. 10, the data seems to suggest a lower plateau length $\bar{\lambda}_1$ for duplex grades.

Table 9. Average and standard deviation of the design-to-numerically computed buckling resistance (an average value lower than 1.0 shall indicate safe predictions)

Buckling type/α and $\bar{\lambda}_0$	Average	Standard deviation	No. of data points with $\bar{\lambda} > \bar{\lambda}_0$
Minor axis buckling/0.49 and 0.2	1.08	0.14	239
Minor axis buckling/0.76 and 0.2	1.01	0.13	239
Major axis buckling/0.49 and 0.2	0.93	0.11	119
Flexural-torsional buckling/0.34 and 0.2	0.98	0.19	50
Minor axis buckling according to AS/NZS standard	0.91	0.11	239

PROOF ONLY

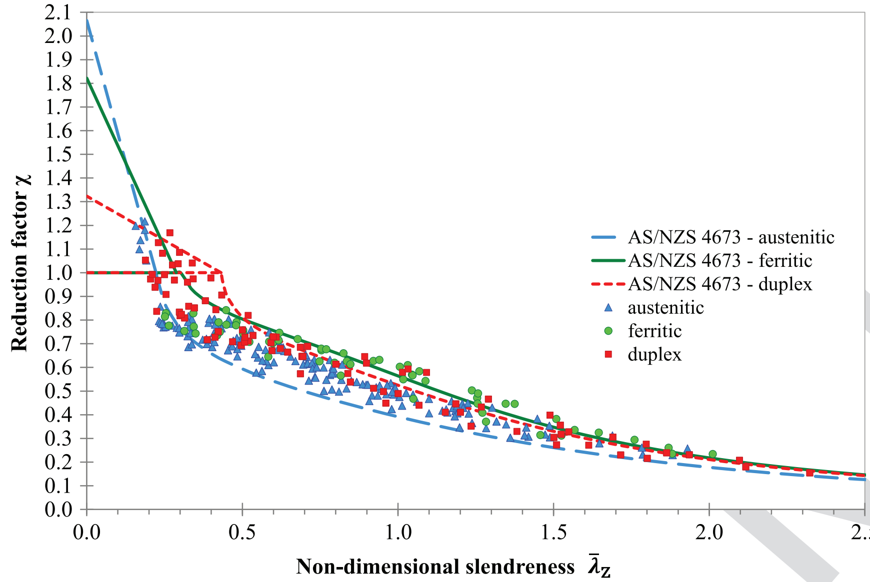

Fig. 10. Comparison of the numerically computed data with the AS/NZS buckling curves for flexural buckling of lipped–channel section columns—minor axis buckling.

In Fig. 10, for slenderness values lower than the plateau length, it was decided to use the formulation proposed in Rossi and Rasmussen (2013) in which strain-hardening effects are accounted for. Therefore, instead of using the classical horizontal yield limit proposed in conventional approaches, a compression level equal to f_u (the tensile strength) is assumed to be attained as the slenderness approaches zero. Thus, the maximum reduction factor χ equals f_u/f_y, which improves the comparison between the design and numerical strengths.

To evaluate the influence of the shift of the centroid when considering the effective cross-section, the data points related to slender cross-sections (Class 4) were selected and reassessed based on the EN 1993-1-4 interaction formulae. The direction of the predicted shift in lipped–channel section leads to a secondary minor axis bending moment $M_{z,pred} = N_{u,pred}e_{Nz}$ with no secondary major axis bending moment. Yield occurs in the cross-section web or lips, depending on the sign of the shift e_{Nz}—i.e., toward the lips or the web—which depends on the cross-section geometry (flange-to-web ratio and section wall slenderness). Table 10 compares the numerically predicted ultimate loads N_u to the Eurocode 3 and AS/NZS design predictions $N_{u,pred,shift}$, considering the shift of the centroid, which were obtained using Eqs. (12) and (24), respectively. In addition, Fig. 11 presents the ratio of the numerical-to-predicted capacity versus the column slenderness $\bar{\lambda}_z$, considering all different buckling curves.

In general, the EN 1993-1-4 interaction in Eq. (12) in conjunction with the suitable buckling curve provides a lower prediction accuracy with higher data scatter but with conservative and safe

Table 10. Comparison of the compression plus uniaxial bending numerical results with the predicted ones (an average value lower than 1.0 shall indicate safe predictions)

Code	Stainless steel grade	Dataset	Buckling factors	Number of data points	Average	Standard deviation
EN 1993-1-4, Eq. (12)	Austenitic	Minor axis FB and minor axis bending	$\alpha = 0.49$ $\bar{\lambda}_0 = 0.2$	80	1.104	0.13
			$\alpha = 0.76$ $\bar{\lambda}_0 = 0.2$	80	1.001	0.12
	Duplex		$\alpha = 0.49$ $\bar{\lambda}_0 = 0.2$	40	0.924	0.11
			$\alpha = 0.76$ $\bar{\lambda}_0 = 0.2$	40	0.825	0.11
	Ferritic		$\alpha = 0.49$ $\bar{\lambda}_0 = 0.2$	42	0.974	0.09
			$\alpha = 0.76$ $\bar{\lambda}_0 = 0.2$	42	0.871	0.09
	All grades	Flexural-torsional buckling and minor axis bending	$\alpha = 0.34$ $\bar{\lambda}_0 = 0.2$	50	0.748	0.18
*	All grades	Major axis FB and minor axis bending	$\alpha = 0.49$ $\bar{\lambda}_0 = 0.2$	63	0.835	0.16
			$\alpha = 0.76$ $\bar{\lambda}_0 = 0.2$	63	0.811	0.16
	Austenitic	Minor axis FB and minor axis bending	$\alpha^* = 1.59$ $\bar{\lambda}_0^* = 0.55$	80	0.828	0.07
	Duplex		$\alpha^* = 1.16$ $\bar{\lambda}_0^* = 0.42$	40	0.921	0.11
	Ferritic		$\alpha^* = 0.94$ $\bar{\lambda}_0^* = 0.56$	42	0.979	0.09
AS/NZS 4673:2001, Eq. (24)	Austenitic	Minor axis FB and minor axis bending	$\alpha^* = 1.59$ $\bar{\lambda}_0^* = 0.55$	80	0.830	0.07
	Duplex		$\alpha^* = 1.16$ $\bar{\lambda}_0^* = 0.42$	40	0.910	0.11
	Ferritic		$\alpha^* = 0.94$ $\bar{\lambda}_0^* = 0.56$	42	0.972	0.10

Note: *New recommendation.

PROOF ONLY

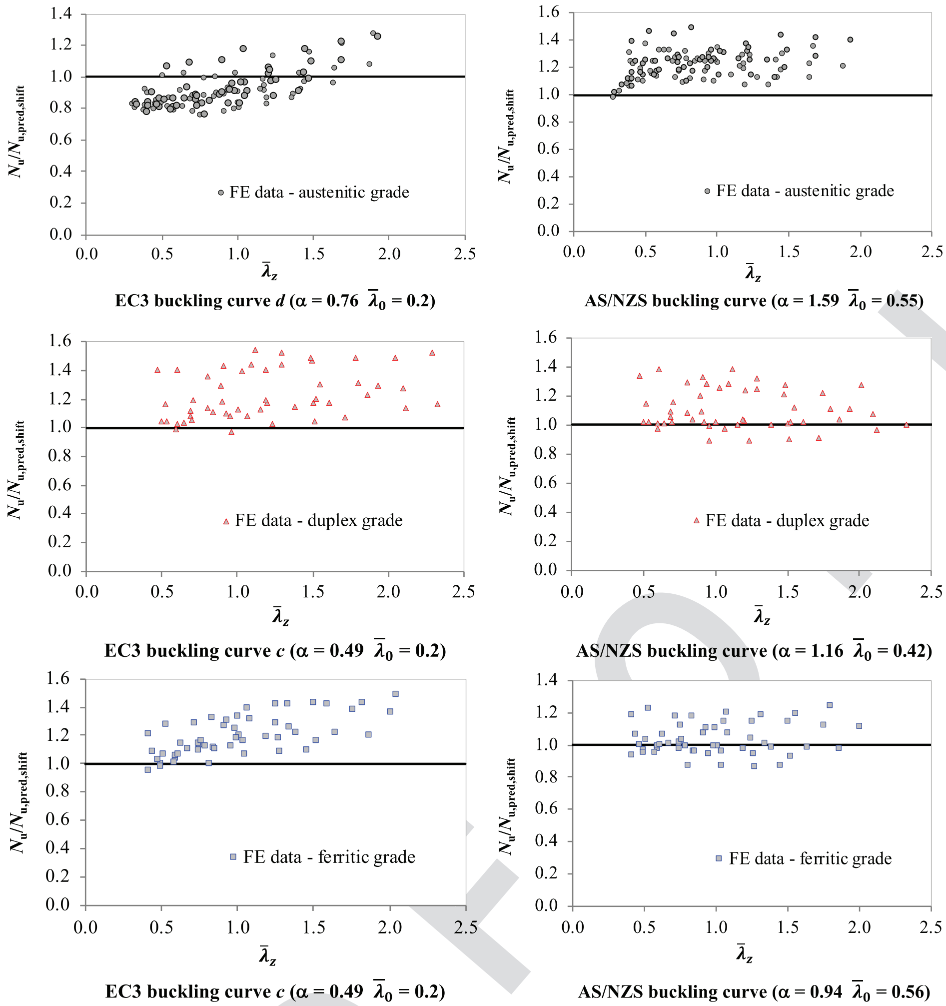

Fig. 11. Comparison of the minor axis FB plus minor axis bending moment numerical capacity with the EN 1993-1-4 predictions considering different buckling curves.

results for stainless steel lipped-channels. Considering minor axis flexural buckling and minor axis bending interaction, an acceptable agreement is achieved between the numerically obtained and the Eurocode 3 predicted capacities for duplex and ferritic stainless steel lipped–channel columns (Table 10). However, the comparison between the numerical data and the codified ones for both buckling curves *c* and *d* in conjunction with a limiting slenderness of 0.2 reveals considerably unsafe predictions in the low and, partially, in the intermediate slenderness range for the austenitic grade (Fig. 11), even though the mean resistance ratios are 1.104 and 1.001, with standard deviations of 0.13 and 0.12.

Both buckling curves *c* and *d* seem suitable in conjunction with the interaction formula for major axis flexural buckling and secondary minor axis bending moment for all stainless steel grades.

But the assessment of the interaction between the axial force and minor axis bending moment in the case of flexural-torsional buckling shows a significantly higher scatter in conjunctions with higher level of conservativeness.

Again, in comparison with Eurocode 3, the AS/NZS design procedure represented by Eq. (24) provides better predictions of the axial load and minor axis bending moment interaction with a lower scatter.

Most importantly, based on the previous reassessment of the Class 4 section, we can conclude that the influence of the centroidal shift is overall rather low. It can be clearly seen from Fig. 12 in which the ratio of the design column capacity $N_{u,\mathrm{pred,\,shift}}$ considering the shift of the effective centroid (minor axis FB plus minor axis bending moment)-to-the-design column capacity $N_{u,\mathrm{pred}}$ (minor axis FB) against the column slenderness $\bar{\lambda}_z$ is depicted. For the austenitic grades, the mean value of IDEM $N_{u,\mathrm{pred,\,shift}}/N_{u,\mathrm{pred}}$ ratio is 0.970, and the CoV is 0.025; for the duplex grade, it is 0.924 and 0.042 respectively, while for the ferritic grade, the mean value is 0.974, and the CoV is 0.017.

Reliability Assessment

Safety Factor γ_m

The following reliability analysis was made for lipped–channel section columns failing by minor or major axis flexural buckling or flexural-torsional buckling. However, the methodology proposed in Afshan et al. (2015), which is in agreement with the one in EN 1990 Annex D (CEN 2002), is presently used with some modifications in the approach to determine the parameters *c* and *d* for each specific test. Indeed, as opposed to what is proposed in Afshan et al. (2015), the parameter *d* is calculated using Eq. (26)

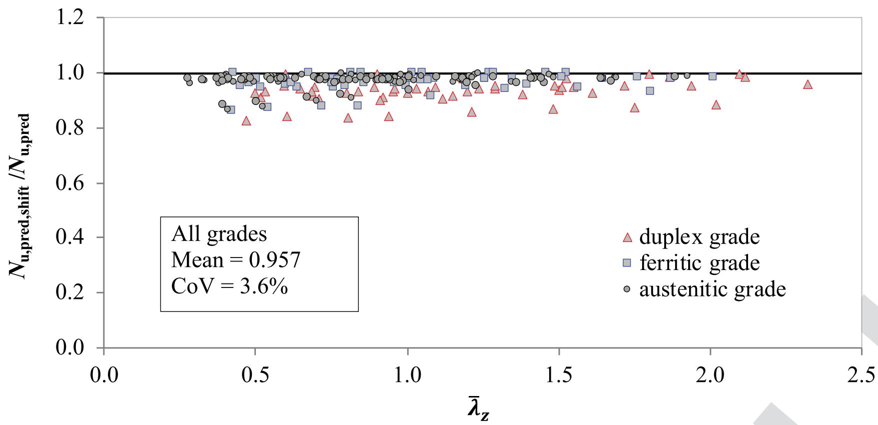

Fig. 12. Reduction of the predicted column capacity $N_{u,\mathrm{pred}}$ caused by the centroid shift of the effective cross-section.

$$d = \frac{\ln\left(\frac{N_{b,Rd,2}}{N_{b,Rd,1}}\right)}{\ln\left(\frac{A_2}{A_1}\right)} \tag{26}$$

where $N_{b,Rd,1}$ and $N_{b,Rd,2}$ are obtained by considering a slight increase of the cross-sectional area A only.

In addition to this modification, the formula for the parameter V_{rt} is taken according to equation D16b of EN 1990:2002 Annex D instead of Eq. (23) of Afshan et al. (2015) where V_{rt} is mentioned instead of V_{rt}^2.

In Afshan et al. (2015), the proposed coefficients of variation for f_y, based on statistical data on material and geometric parameters from stainless steel producers for austenitic, ferritic, and duplex grades are 0.06, 0.045, and 0.03, respectively. The coefficient of variation of the geometric properties is considered equal to 0.05, and this value was utilized for stainless steel in the development of the AISC stainless steel design guide (AISC 2013).

In the present analysis, the total test population was divided into appropriate subsets depending on the considered group of data, respectively, for flexural (minor or major) or flexural-torsional buckling, on the cross-section class (if Class 4) and stainless steel family. Clause D.8.2.2.5 of EN 1990 Annex D was then used. It allows the use of the total number of tests in the original series for determining the fractile factor to avoid large safety factors due to a low amount of data points in each subset, even though the number of data points presently remained high for each subset.

The results of this analysis are presented in Table 11, where n is the total number of data points (tests or FE results); b is the average experimental (or FE)-to-model resistance ratio based on a least squares fit of the slope of the r_{ei} versus r_{ti} plot for each set of data [Eq. (27)]; the coefficient of variation V_δ of the error term $\delta_i = r_{ei}/br_{ti}$ is used as a measure of the variabilities of the predictions obtained from the resistance function; the coefficient of variation V_{rt} accounts for the effect of the variability of the basic variables, including material and geometric properties; and γ_{M1} is the partial safety factor for the resistance against buckling. Note that the analyses carried out in this paper follow the recommendations of Afshan et al. (2015). However, to calculate the safety factors, the procedure proposed in the Annex D in conjunction with the formula (6.6c) is used in which the safety factor is directly obtained from the characteristic value of the member resistance r_{ki}. Afshan et al. (2015) propose to use the overstrength factors in the evaluation of the safety factor, the effect of which will be discussed in the last section of this paper

$$b = \sum_{i=1}^{n} \frac{r_{ei} r_{ti}}{r_{ti}^2} \tag{27}$$

Considering all data points together, without a distinction of the stainless steel family, leads to safety factors higher than 1.10 regardless of the chosen buckling curve and even when Class 4 cross-sections are excluded from the analysis. It is probably due to two factors: (1) the simplified design procedure provided in EN 1993-1-3, Clause 5.5.3, and combined with (2) inappropriate buckling curves; however, there is presently no clear evidence of that.

Table 11. Results of the reliability assessment for EN 1993-1-4—design-to-numerically computed buckling resistances according to EN 1993-1-4 (CEN 2015)

Buckling type/α and $\bar{\lambda}_0$	Average	Standard deviation	n number of data points with $\bar{\lambda} > \bar{\lambda}_0$	b	V_δ	γ_m
Minor axis buckling/0.49 and 0.2	1.08	0.14	239	—	—	—
• Without class 4	1.01	0.12	77	0.9695	0.1215	1.143
• Duplex—all classes	1.04	0.13	56	0.9331	0.1278	1.142
• Ferritic—all classes	1.02	0.13	58	0.9426	0.1255	1.144
Minor axis buckling/0.76 and 0.2	1.01	0.13	239	—	—	—
• Austenitic HR—all classes	1.06	0.11	79	0.9185	0.1074	1.133
• Austenitic CR—all classes	1.04	0.13	75	0.9316	0.1218	1.145
Major axis buckling/0.49 and 0.2	0.93	0.11	119	—	—	—
• Without class 4	0.95	0.11	56	0.9992	0.1261	1.158
Flexural-torsional buckling/0.34 and 0.2	0.98	0.19	50	0.9098	0.2034	1.244

Note: HR = hot-rolled strip; and CR = cold-rolled strip.

PROOF ONLY

However, Table 11 reveals that the safety factors remain acceptable as long as the cross-section is not of Class 4, in which case it leads to very unsatisfactory and/or unconservative results. Note that only 77 cross-sections are of a different class than Class 4.

For minor axis buckling, buckling curve c ($\alpha = 0.49$) leads to the lowest safety factors for ferritic and duplex grades (including Class 4 cross-sections) but are still higher than 1.10 (Table 11). Note that the fact that buckling curve c seems more adequate to predict the behavior of ferritic stainless steel is not in agreement with the current proposal in the *Design Manual for Structural Stainless Steel* (Afshan et al. 2017). However, the introduction of the overstrength factors in combination with an evaluation of the safety factors as the ratio of the nominal resistance r_{ni} to the design resistance r_{di} reveals an even higher safety factor (than the ones presented in Table 11), finally excluding the use of buckling curve c.

For austenitic grades, the comparison between the normalized FE buckling loads and the codified ones reveals an unsafe prediction in the low and partially intermediate slenderness range but conservative prediction in the high slenderness range (for a slenderness higher than about 1.20). However, buckling curve d, be it for Class 4 or not, provides unsatisfactory results leading to high safety factors, be it with or without the inclusion of the overstrength factor.

For major axis buckling, buckling curve c again leads to the lowest safety factors as long as Class 4 cross-sections are excluded, leaving only 56 relevant data points. The safety factor is nonetheless still higher than 1.10 (be it with or without the inclusion of the overstrength factor) (Table 11).

For the flexural-torsional buckling mode, due to a higher scatter of the data, the safety factor increases. However, the number of data points is low, and the flexural-torsional buckling mode found in the FE investigations was, most of the time, coupled with other buckling modes.

In addition, the existing design model does not always give an accurate prediction of the failure mode, especially for columns with slender cross-sections: the obtained FE failure mode was generally flexural-buckling about the minor axis while the code would predict a flexural-torsional buckling mode.

To conclude, it seems that regardless of the considered buckling mode or class, the parameters α and $\bar{\lambda}_0$ currently adopted in EN 1993-1-4, which are respectively equal to 0.49 and 0.4, should be revised.

Resistance Factor ϕ_c

The resistance factors to be used in conjunction with the AS/NZS rules have been calculated using the statistics shown in Tables 1 and 2, and the LRFD framework, e.g., see Section F.1.1 of the North American Specification AISI-S100 (AISI 2016). Considering the dead and live load combination, the resistance factors are determined

$$\phi_c = C_\phi (M_m F_m P_m) e^{-\beta_0 \sqrt{V_M^2 + V_F^2 + C_P V_P^2 + V_Q^2}} \tag{28}$$

where $C_\phi = 1.52$, for LRFD is the calibration coefficient; $M_m = 1.1$ and $F_m = 1.0$ are the mean values of the random material (M) and fabrication (F) factors for concentrically loaded compression members, respectively; $V_M = 0.1$ and $V_F = 0.05$ are the CoVs of these factors; $\beta_0 = 2.5$ is the target reliability index for LRFD for structural members; P_m and V_P are the mean and CoV of the professional factor (P), shown as the test-to-design strength ratio; $V_Q = 0.21$ is the CoV of the load effect; and C_P is the correction factor calculated

Table 12. Results of the reliability assessment for AS/NZS 4673:2001

Group	P_m	V_P	n	ϕ_c
All data	1.11	0.12	239	0.96
• Austenitic HR	1.18	0.07	65	1.06
• Austenitic CR	1.24	0.08	60	1.11
• Duplex	1.03	0.09	53	0.91
• Ferritic	1.00	0.06	61	0.90

$$C_P = \begin{cases} \left(1 + \frac{1}{n}\right) \frac{m}{m-2} & \text{for } n \geq 4 \\ 5.7 & \text{for } n = 3 \end{cases} \tag{29}$$

where $m = n$-1 is the degrees of freedom; and n = number of tests.

The resistance factors ϕ_c are included in Table 12 and indicate that the reliability is sensitive to how the test-to-design strength data are grouped. Taking into account all available test data, the resistance factor is always higher than 0.9, which is the current value of ϕ_c for a column design based on the explicit calculation of N_{ce}, as per AS/NZS 4673:2001 (AS/NZS 2001). It is in essence due to the particular shape of the buckling curve, which is able to tackle quite well the behavior in the low and medium slenderness range as well as the dependency to the family of stainless steel, as can be seen in Fig. 10.

It can also be concluded from Fig. 10 that for slenderness values lower than the plateau length, the formulation proposed in Rossi and Rasmussen (2013) in which strain-hardening effects are considered through the use of a maximum compression level equal to f_u provides good predictions.

Conclusion

In conclusion, for minor axis buckling of lipped–channel section columns, we recommend the use of different column curves per family of stainless steel as well as the revision of the current parameters α and $\bar{\lambda}_0$ currently adopted in EN 1993-1-4, which are respectively equal to 0.49 and 0.4.

Seeing the very good agreement found against the AS/NZS guidance, we shall conclude by proposing that the factor η, currently being the linear expression given in Eq. (30) in the European guidance Eq. (7), shall be replaced by Eq. (23) with the values of α^*, β, $\bar{\lambda}_0{}^*$, and $\bar{\lambda}_1$ from Table 3

$$\eta = \alpha(\bar{\lambda} - \bar{\lambda}_0) \tag{30}$$

In this case, the safety factors γ_m as per EN 1990:2002 Annex D, based on the characteristic resistance r_{ki} are 1.147, 1.112, or 1.091, respectively, for austenitic, duplex, and ferritic grades. We should mention that the introduction of overstrength factors in combination with the use of the nominal resistance r_{ni} in place of the characteristic resistance leads to a slightly higher safety factor for the duplex family (lower than 1.10 for the austenitic and ferritic families), which indicates that further study is needed to either confirm an overstrength factor of 1.1 and/or the values of the parameters α^*, β, $\bar{\lambda}_0{}^*$, and $\bar{\lambda}_1$ in Table 3 for the duplex family. It is also worth noting that, for duplex, the reliability assessment is based on 53 points, 30 of which have a slenderness higher than 1.0, and so the overstrength factor has little effect.

It is also important to mention that the use of the recommended factor η given in Eq. (23) in conjunction with the European guidance also provides considerably precise and reliable predictions of the column strength when the shift of the centroid of the effective

PROOF ONLY

cross-section is taken into account, as can be seen in Table 10 (lines labeled with α^*).

Acknowledgments

This investigation is supported by the Serbian Ministry of Education, Science, and Technological Development through the TR-36048 project.

References

Afshan, S., I. Arrayago, N. Baddoo, L. Gardner, G. Gedge, M. Jandera, E. Real, B. Rossi, N. Stranghöner, and O. Zhao. 2017. *Design manual for structural stainless steel*. London: Steel Construction Institute.

Afshan, S., P. Francis, N. R. Baddoo, and L. Gardner. 2015. "Reliability analysis of structural stainless steel design provisions." *J. Constr. Steel Res.* 114 (Nov): 293–304. https://doi.org/10.1016/j.jcsr.2015.08.012.

AISC. 2013. *Design guide 27: Structural stainless steel*. Chicago: AISC.

AISI (American Iron and Steel Institute). 2016. *North American specification for the design of cold-formed steel structural members*. AISI-S100. Washington, DC: AISI.

Arrayago, I., E. Real, and L. Gardner. 2015. "Description of stress–strain curves for stainless steel alloys." *Mater. Des.* 87 (Dec): 540–552. https://doi.org/10.1016/j.matdes.2015.08.001.

AS/NZS (Australian Standard/New Zealand Standard). 2001. *Cold-formed stainless steel structures*. AS/NZS 4673:2001. Sydney, Australia: Standards Australia.

Becque, J., M. Lecce, and K. J. R. Rasmussen. 2008. "The direct strength method for stainless steel compression members." *J. Constr. Steel Res.* 64 (11): 1231–1238. https://doi.org/10.1016/j.jcsr.2008.07.007.

Becque, J., and K. J. R. Rasmussen. 2009a. "A numerical investigation of local–overall interaction buckling of stainless steel lipped channel columns." *J. Constr. Steel Res.* 65 (8–9): 1685–1693. https://doi.org/10.1016/j.jcsr.2009.04.027.

Becque, J., and K. J. R. Rasmussen. 2009b. "Experimental investigation of local-overall interaction buckling of stainless steel lipped channel columns." *J. Constr. Steel Res.* 65 (8–9): 1677–1684. https://doi.org/10.1016/j.jcsr.2009.04.025.

CEN (European Committee for Standardization). 2002. *Eurocode: Basis of structural design*. EN 1990. Brussels, Belgium: CEN.

CEN (European Committee for Standardization). 2004. *Eurocode 3: Design of steel structures, Part 1-3: General rules—Supplementary rules for cold-formed members and sheeting*. EN 1993-1-3. Brussels, Belgium: CEN.

CEN (European Committee for Standardization). 2006. *Eurocode 3: Design of steel structures, Part 1-5: Plated structural elements*. EN 1993-1-5. Brussels, Belgium: CEN.

CEN (European Committee for Standardization). 2008. *Execution of steel structures and aluminium structures—Part 2: Technical requirements for the execution of steel structures*. EN 1090-2. Brussels, Belgium: CEN.

CEN (European Committee for Standardization). 2015. *Eurocode 3: Design of steel structures, Part 1-4: General rules—Supplementary rules for cold-formed members and sheeting*. EN 1993-1-4. Brussels, Belgium: CEN.

Dobrić, J., D. Budjevac, Z. Marković, and N. Gluhović. 2017. "Behaviour of stainless steel press-braked channel sections under compression." *J. Constr. Steel Res.* 139 (Dec): 236–253. https://doi.org/10.1016/j.jcsr.2017.09.005.

Dobrić, J., M. Pavlović, Z. Marković, D. Buđevac, and M. Spremić. 2018. "Resistance of cold-formed built-up stainless steel members—Part II: Numerical simulation." *J. Constr. Steel Res.* 140 (Jan): 247–260. https://doi.org/10.1016/j.jcsr.2017.10.032.

Gardner, L., and D. A. Nethercot. 2004. "Numerical modeling of stainless steel structural components a consistent approach." *J. Struct. Eng.* 130 (10): 1586–1601. https://doi.org/10.1061/(ASCE)0733-9445(2004)130:10(1586).

Kuwamura, H. 2003. "Local buckling of thin-walled stainless steel members." *Steel Struct.* 3: 191–201.

Lecce, M. 2006. "Distortional buckling of stainless steel sections." Ph.D. thesis, Dept. of Civil Engineering, Univ. of Sydney.

Lecce, M., and K. J. R. Rasmussen. 2004. *Experimental investigation of the distortional buckling of cold-formed stainless steel sections*. Research Rep. No R844. Sydney, Australia: Univ. of Sydney.

Lecce, M., and K. J. R. Rasmussen. 2006. "Distortional buckling of cold-formed stainless steel sections: Experimental investigation." *J. Struct. Eng.* 132 (4): 497–504. https://doi.org/10.1061/(ASCE)0733-9445(2006)132:4(497).

Rasmussen, K. J. R., and G. J. Hancock. 1993. "Design of cold-formed stainless steel tubular members I: Columns." *J. Struct. Eng.* 119 (8): 2349–2367. https://doi.org/10.1061/(ASCE)0733-9445(1993)119:8(2349).

Rasmussen, K. J. R., and J. Rondal. 1997. "Explicit approach to design of stainless steel columns." *J. Struct. Eng.* 123 (7): 857–863. https://doi.org/10.1061/(ASCE)0733-9445(1997)123:7(857).

Rasmussen, K. J. R., and J. Rondal. 2000. "Column curves for stainless steel alloys." *J. Constr. Steel Res.* 54 (1): 89–107. https://doi.org/10.1016/S0143-974X(99)00095-4.

Rossi, B., S. Afshan, and L. Gardner. 2013. "Strength enhancements in cold-formed structural sections—Part II: Predictive models." *J. Constr. Steel Res.* 83 (Apr): 189–196. https://doi.org/10.1016/j.jcsr.2012.12.007.

Rossi, B., J.-P. Jaspart, and K. J. R. Rasmussen. 2010. "Combined distortional and overall flexural-torsional buckling of cold-formed stainless steel sections: Experimental investigations." *J. Struct. Eng.* 136 (4): 354–360. https://doi.org/10.1061/(ASCE)ST.1943-541X.0000130.

Rossi, B., and K. J. R. Rasmussen. 2013. "Carrying capacity of stainless steel columns in the low slenderness range." *J. Struct. Eng.* 139 (6): 1088–1092. https://doi.org/10.1061/(ASCE)ST.1943-541X.0000666.

Saliba, N., and L. Gardner. 2013. "Experimental study of the shear response of lean duplex stainless steel plate girders." *Eng. Struct.* 46 (Jan): 375–391. https://doi.org/10.1016/j.engstruct.2012.07.029.

Schafer, B. W., and T. Pekoz. 1998. "Computational modeling of cold-formed steel: Characterizing geometric imperfections and residual stresses." *J. Constr. Steel Res.* 47 (3): 193–210. https://doi.org/10.1016/S0143-974X(98)00007-8.

Schepens, M. 2008. "Etude de profilés à parois minces en acier inoxydable." [In French.] Graduation thesis, Dept. of Civil Engineering, Univ. of Liège.

PROOF ONLY